Prolonged Kelvin–Helmholtz Waves at Dawn and Dusk Flank Magnetopause: Simultaneous Observations by *MMS* and *THEMIS*

S. W. Lu[1,2], C. Wang[1,2], W. Y. Li[1,3], B. B. Tang[1], R. B. Torbert[4], B. L. Giles[5], C. T. Russell[6], J. L. Burch[7], J. P. McFadden[8], H. U. Auster[9], and V. Angelopoulos[10]

[1] State Key Laboratory of Space Weather, National Space Science Center, Chinese Academy of Sciences, Beijing 100190, People's Republic of China
cw@spaceweather.ac.cn, wyli@spaceweather.ac.cn
[2] University of Chinese Academy of Sciences, Chinese Academy of Sciences, Beijing 100049, People's Republic of China
[3] Swedish Institute of Space Physics, Uppsala, Sweden
[4] Space Science Center, University of New Hampshire, Durham, NH, USA
[5] NASA Goddard Space Flight Center, Greenbelt, MD, USA
[6] Institute of Geophysics and Planetary Physics, University of California, Los Angeles, CA, USA
[7] Southwest Research Institute, San Antonio, TX, USA
[8] Space Science Laboratory, University of California, Berkeley, CA, USA
[9] Institut für Geophysik und extraterrestrische Physik der Technischen Universität Braunschweig, Mendelssohnstrasse 3, D-38106 Braunschweig, Germany
[10] Institute of Geophysics and Planetary Physics, University of California, Los Angeles, CA, USA

Abstract

The Kelvin–Helmholtz (K-H) waves predominantly excited at the Earth's low-latitude magnetopause were suggested to be dawn–dusk asymmetric. We report a prolonged simultaneous observations of the K-H waves on the dawn and dusk magnetopause by *Magnetospheric Multiscale* (*MMS*) and *THEMIS-A* (*THA*) spacecraft, respectively. The quasi-periodic K-H waves on both flanks have unambiguous low-density and high-speed patterns. The wave periods vary gradually on both flanks, with similar average periods (303 ± 107 s for *MMS* and 266 ± 102 s for *THA*). The lag time between the variations of the wave periods is close to the wave propagation time from *THA* to *MMS*, which suggests that the K-H waves generate and propagate quasi-symmetrically on both flanks. Larger local magnetic shear angles are observed on the trailing edges by *MMS* than by *THA*, which is probably due to the strong magnetic field distortion during the tailward propagation. The increased magnetic shear may excite magnetic reconnection, thus contributing to the formation of the low-latitude boundary layer.

Key words: plasmas – waves

1. Introduction

The Kelvin–Helmholtz (K-H) instability could be excited at a plasma boundary where large velocity shear exists. The K-H waves have been widely studied in various plasma environments, including solar corona (Foullon et al. 2011), magnetosphere (e.g., Hasegawa et al. 2004), and potentially in heliospheric boundaries (Borovikov & Pogorelov 2014). The unstable condition of the K-H instability can be satisfied at the flank magnetopause where the fast-moving anti-sunward magnetosheath flow meets the quasi-stagnant magnetosphere plasma (Chandrasekahar 1961). The K-H instability is considered to be an important mechanism for the transport of solar wind particles and energy into the Earth's magnetosphere (Hasegawa et al. 2004, 2009; Fairfield et al. 2007). Both numerical simulations (Nykyri & Otto 2001; Nakamura & Fujimoto 2005; Nakamura et al. 2013, 2017) and in situ observations (Hasegawa et al. 2009; Eriksson et al. 2016; Li et al. 2016) have shown that the magnetic reconnection induced by the K-H waves breaks the frozen-in condition of plasma during the large-scale evolution of the waves, allowing plasma transport from the solar wind into the magnetosphere.

The K-H unstable condition is more likely to be satisfied if plasma on the boundary has large velocity shear and magnetic fields are perpendicular to propagating direction (Chandrasekahar 1961). Previous works have shown that the K-H waves are more likely to be excited under northward interplanetary magnetic field (IMF; Miura 1995; Farrugia et al. 1998; Guo et al. 2010) and fast solar wind speed (Otto & Fairfield 2000; Li et al. 2013; Kavosi & Raeder 2015), although a few K-H events during southward IMF have been reported (Hwang et al. 2011; Yan et al. 2014). The relationships between solar wind conditions and properties of the K-H waves have also been extensively studied (e.g., Farrugia et al. 1998, 2003; Li et al. 2013; Lin et al. 2014). A comprehensive statistical study by Lin et al. (2014) shows that periods of the K-H waves decrease with solar wind speed, while they increase with the clock angle of IMF. During the convective propagation of the K-H waves from dayside to nightside magnetopause, the wavelengths and the phase speeds gradually increase (Li et al. 2012; Lin et al. 2014), and the waves themselves develop from a quasi-linear to nonlinear stage, generating rolled-up vortices around the leading edges of the K-H waves (Hasegawa et al. 2004, 2006; Takagi et al. 2006) that distort the local magnetic fields and create conditions for magnetic reconnection (e.g., Nykyri & Otto 2001).

The transport of magnetosheath plasma contributes to the formation of the cold dense plasma sheet (CDPS) adjacent to the magnetopause boundary layer under prolonged northward IMF (e.g., Terasawa et al. 1997). The plasmas of magnetosheath origin inside the CDPS are denser and hotter by 30%–40% at the dawnside than the duskside (Wing et al. 2005). The dawn–dusk asymmetry of ion temperatures of magnetosheath plasma is inadequate for the asymmetric CDPS

(Dimmock et al. 2015), which suggests that the asymmetry of the K-H waves may contribute to the asymmetric CDPS. The distributions of the K-H waves have been extensively studied. For example, Taylor et al. (2012) pointed out that about 62% of the K-H waves (21 out of 34) are found on the duskside, while Lin et al. (2014) found no clear asymmetry in a collection of 56 K-H waves. Moreover, a recent study by Henry et al. (2017) has shown that the K-H waves have preference on the dawnside during Parker-spiral IMF. The mechanism is suggested to be the asymmetric K-H growth rate at both flanks (Nykyri 2013).

The multispacecraft observations can help us understand the K-H waves simultaneously propagating at both flanks (Nishino et al. 2011; Ling et al. 2018). In this paper, we report a case study of the prolonged K-H waves observed simultaneously on the dawn and dusk magnetopause by the *Magnetospheric Multiscale* (*MMS*; Burch et al. 2015) and *Time History of Events and Macroscale Interactions during Substorms* (*THEMIS*; Angelopoulos 2008) spacecraft. The symmetry and correlations of the K-H waves on both flanks are analyzed in detail.

2. Instruments

The in situ measurements of plasma and magnetic field from *MMS* and *THEMIS* spacecraft are used in this paper. For *MMS* data, we use the fast-mode (4.5 s) and burst-mode (0.15 s) ion data from the Fast Plasma Investigation (Pollock et al. 2016) and the survey-mode (16 Hz) magnetic field data from Fluxgate Magnetometer (FGM; Torbert et al. 2014). For *THEMIS* data, we use ion data from the Electrostatic Analyzer (McFadden et al. 2008) and magnetic field data from the FGM (Auster et al. 2008), both sampled at the spin resolution (3 s). The vectors are presented in the Geocentric Solar Magnetospheric (GSM) coordinate system. High-resolution (1 minute) OMNI data are used to get the solar wind and IMF parameters.

During the time interval of interest, *MMS* is located at the dawnside magnetopause. The average distance of four *MMS* spacecraft is about 50 km, which is much smaller than the typical wavelengths of the K-H waves (several R_E; see Lin et al. 2014). Thus, the *MMS* observations of this event are shown representatively by *MMS1* data. Meanwhile, three of the five *THEMIS* spacecraft (A, D, and E) are located at the duskside magnetopause, in which *THEMIS-A* (*THA*) spacecraft has the longest simultaneous observation with *MMS*. The following sections provide detailed analysis of the K-H waves by *MMS* and *THA*.

3. Observations

### 3.1. K-H Waves Observed by MMS and THA

The K-H waves at the Earth's magnetopause are characterized by quasi-periodic fluctuations of the plasma and magnetic field parameters. We adopt the empirical criteria proposed by Hasegawa et al. (2006) to identify the K-H wave events from the in situ measurements: (1) The plasma and the magnetic field on the magnetosheath side of the magnetopause and/or that in the upstream solar wind are quasi-steady, and the orientation of the magnetic field is northward throughout the time interval of interest. (2) The fluctuations of the plasma and magnetic field parameters during the magnetopause boundary crossings are quasi-periodic with periods between 1 and 5 minutes. (3) The low-density and high-speed (LDHS) pattern (Takagi et al. 2006) has sufficient data points with density less than half of

that on the magnetosheath side and anti-sunward speed higher than that of the magnetosheath plasma.

Figures 1(a)–(d) show the solar wind condition during the interval of 04:00–08:00 UT on 2017 May 29. The solar wind and IMF conditions are generally quasi-steady during this time. The average solar wind speed is $346 \, \text{km s}^{-1}$. The dynamic pressure is around 2.8 nPa with a few pulses. The IMF has a strong B_y component of about 10 nT, while the B_z component holds northward most of the time, with a varying amplitude from -1 to 6 nT. The IMF clock angle $\phi = \tan^{-1} B_y/B_z$ varies between 30° and 102°, with an average clock angle of 70°.

The trajectories of *MMS* and *THA* spacecraft are shown in Figures 1(e)–(f), with magnetopause position given by Shue et al. (1997). *MMS* crossed the dawnside flank magnetopause at $[-15.0, -16.3, 3.5] \, R_E$, while *THA* crossed the duskside magnetopause at $[3.9, 11.7, -3.7] \, R_E$. Plasma and magnetic field data from *MMS* and *THA* spacecraft are shown in Figures 1(g)–(r). The ion bulk velocity and magnetic field data are present in the local LMN coordinates, where N is the magnetopause normal direction determined by the minimum variance direction of the magnetic field, M is the cross product of N and the maximum variance direction of the ion velocity, and L completes the right-handed orthogonal coordinate system, which is approximately opposite to the magnetosheath flow direction. In particular, the three coordinates for *MMS* observations are $\textbf{\textit{L}}_{MMS} = [0.911, 0.387, -0.142]$, $\textbf{\textit{M}}_{MMS} = [0.200, -0.114, 0.973]$, and $\textbf{\textit{N}}_{MMS} = [0.360, -0.915, -0.181]$ in GSM coordinate, and for *THA* observations they are $\textbf{\textit{L}}_{THA} = [0.739, -0.460, -0.492]$, $\textbf{\textit{M}}_{THA} = [0.080, -0.665, -0.742]$, and $\textbf{\textit{N}}_{THA} = [0.669, 0.588, -0.455]$. Quasi-periodic fluctuations in the ion moments and magnetic fields are observed by *MMS* and *THA* during the magnetopause boundary crossings from the hot and tenuous magnetosphere to the cold and dense magnetosheath. The typical periods are roughly estimated to be 3–5 minutes. Detailed analysis of wave periods will be presented in the following section. The time interval of quasi-periodic fluctuations by *MMS* is mainly between 04:30 UT and 07:00 UT, and between 05:00 UT and 07:30 UT for *THA* observations. Thus, the time intervals of the quasi-periodic fluctuations observed by *MMS* and *THA* overlap for about 2 hr. The main differences between the dawn and dusk magnetopause crossings are: (1) The L direction has a large Z component on the duskside, which means that the magnetosheath has a southward flow. This is consistent with the fact that the magnetosheath environments are asymmetric under B_y-dominant IMF (Guo & Wang 2010). (2) The V_L component of the magnetosheath ion flow is larger at the dayside than the nightside. (3) The variations of the total magnetic field amplitude is stronger at the dawnside.

Figures 1(s) and (t) show the scatter plots of N_i versus V_L for the waves on both flanks. In each panel, the top left and the bottom right parts correspond to the magnetosphere and magnetosheath, respectively, while the data points between them correspond to the boundary layer. There are sufficient data points with density less than half of that on the magnetosheath side and speed higher than that of the magnetosheath plasma. These LDHS patterns are consistent with the patterns of the rolled-up vortices shown by Takagi et al. (2006) and Hasegawa et al. (2006), except that the V_L components of the LDHS plasma does not significantly exceed the magnetosheath flow speed. This is probably because the K-H waves have not reached the highly nonlinear stage at the
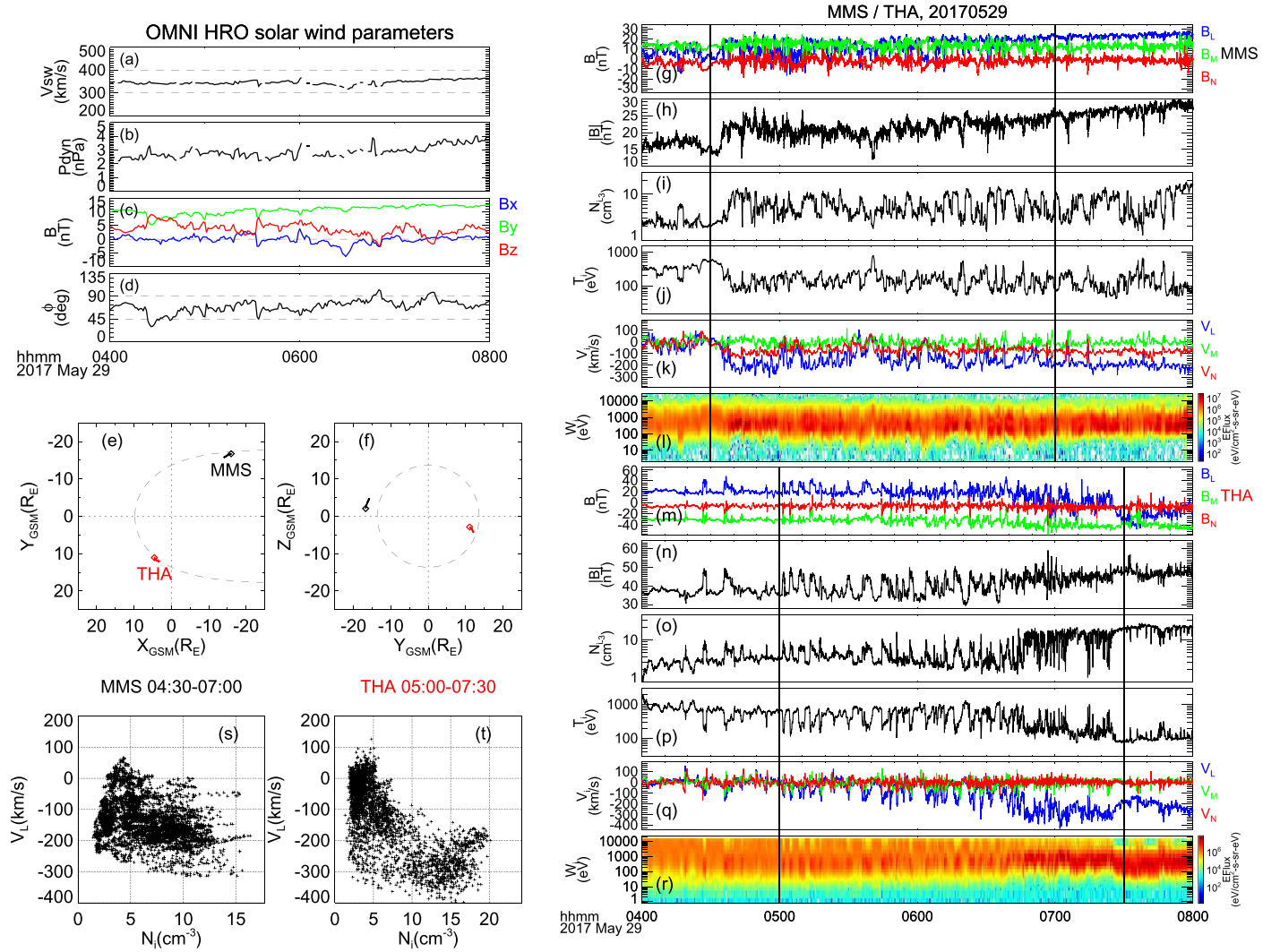
Figure 1. Overview of OMNI, *MMS*, and *THA* data during the interval of 04:00–08:00 UT on 2017 May 29. ((a)–(d)) OMNI solar wind speed, dynamic pressure, IMF, and its clock angle ϕ. ((e)–(f)) *MMS* (black) and *THA* (red) trajectories in GSM *XY* and *YZ* planes. Diamonds represent their respective starting positions. Magnetopause position by Shue et al. (1997) is plotted as the dashed curves. *MMS* observations of (g) $\boldsymbol{B}$ in LMN coordinate, (h) $|\boldsymbol{B}|$, (i) ion number density N_i, (j) ion thermal temperature T_i, (k) ion bulk velocity $\boldsymbol{V}_i$ in LMN coordinate, and (l) ion energy flux. The investigated time interval of the K-H wave (04:30–07:00 UT) is marked by two vertical solid lines. *THA* observations are presented in panels (m)–(r) in the same way as *MMS*. The investigated time interval of the K-H wave (05:00–07:30 UT) is marked by vertical solid lines. ((s)–(t)) Scatter plots of V_L vs. N_i by *MMS* and *THA* during their respective time intervals of the K-H wave events. *MMS* burst data are used in panel (s).

MMS and *THA* locations due to relatively slow solar wind speed during this event.

To sum up, the quasi-periodic fluctuations observed by *MMS* and *THA* satisfy the criteria of the K-H waves proposed by Hasegawa et al. (2006). The following sections will focus on detailed analysis of the boundary conditions and properties of the waves for both events.

3.2. Magnetosphere–Magnetosheath Boundary Conditions of the K-H Waves

To obtain the magnetosphere–magnetosheath boundary conditions for the K-H waves on both flanks, we adopt a transition parameter (Hapgood & Bryant 1992) to label the spatial structure of the K-H waves. The transition parameter τ is defined by

$$\tau = \frac{\log_{10} r - \log_{10} r_{\min}}{\log_{10} r_{\max} - \log_{10} r_{\min}} \times 100, \qquad (1)$$

where $r = N_i/T_i$ is the ratio between the ion number density and the ion temperature. Figures 2(a) and (j) show the scatter plots of ion number density against ion temperature observed by *MMS* and *THA*, respectively. The red lines connect the data points corresponding to the maximum and minimum values of τ, along which all values of τ are given.

Plasma parameters and magnetic fields as functions of τ are presented in Figures 2(b)–(i) and (k)–(r) for *MMS* and *THA*, respectively. The average values and standard deviations of parameters are given for 10 ranges of τ. The data points are divided into magnetosphere, boundary layer, and magnetosheath regions by particular thresholds of τ, which are marked by vertical dashed lines in the panels. The thresholds are determined by the systematical jumps of B_L and V_L parameters in Figure 2. The thresholds of magnetosphere and magnetosheath regions are $\tau = 20$ and $\tau = 70$ for *MMS*, and $\tau = 30$ and $\tau = 70$ for *THA*.
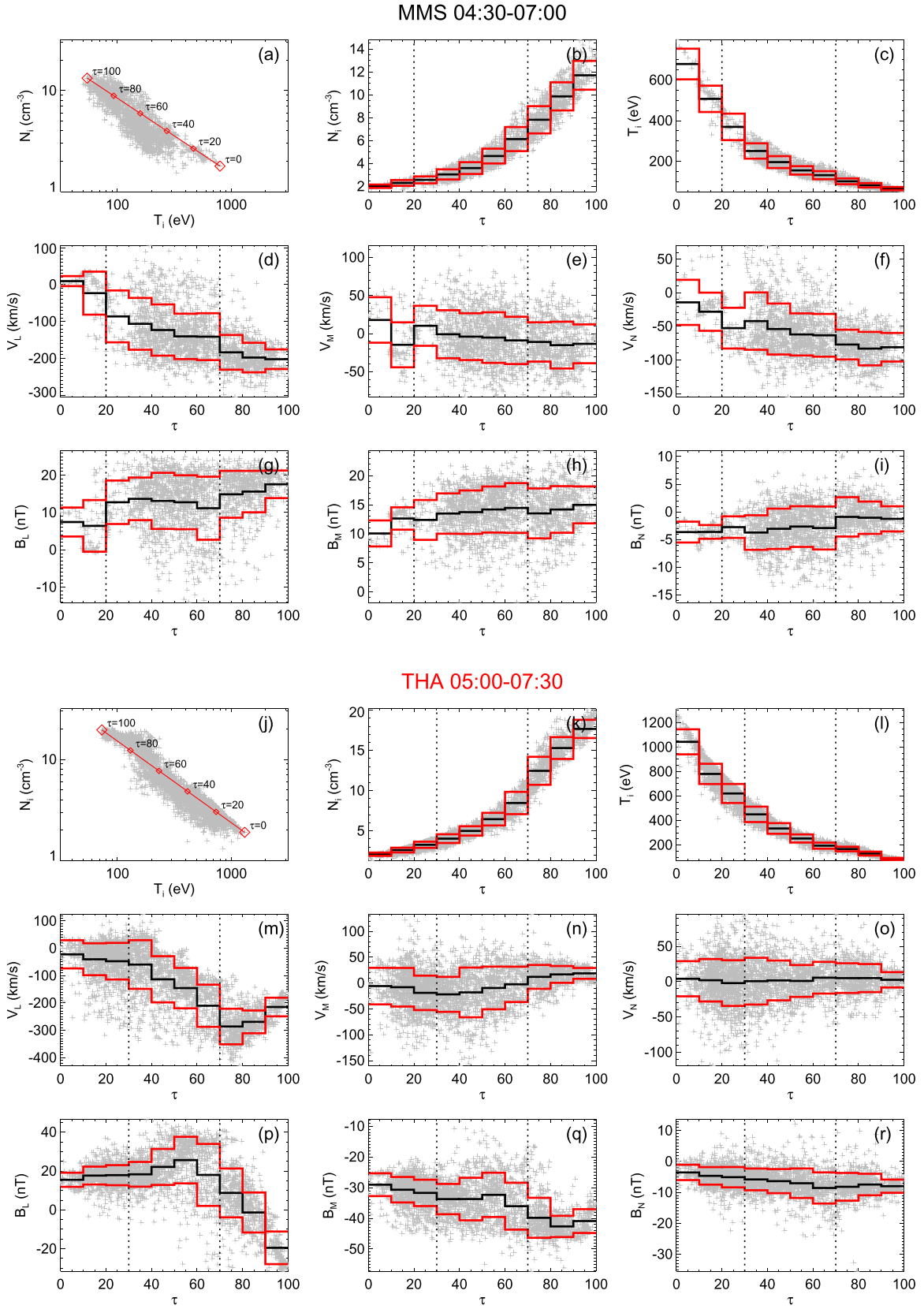
Figure 2. Determination of boundary conditions of the K-H wave events. (a) Scatter plot of N_i vs. T_i by *MMS*. The red line and diamonds denote the transition parameter τ. ((b)–(i)) *MMS* observation of N_i, T_i, V_i, and $\boldsymbol{B}$ as functions of τ. Black and red histograms denote average values and standard deviations for 10 separate ranges of τ. Vertical dashed lines denote thresholds $\tau = 20$ and $\tau = 70$. (j) Scatter plot of N_i vs. T_i by *THA*, in the same way as panel (a). ((k)–(r)) *THA* observations of boundary conditions. Scatter plots and histograms are in the same way as panels (b)–(i). Vertical dashed lines denote thresholds $\tau = 30$ and $\tau = 70$.

Table 1
Magnetosphere–Magnetosheath Boundary Conditions and Properties of the K-H Waves Observed by *MMS* and *THA*

	MMS		*THA*	
	Magnetosphere	Magnetosheath	Magnetosphere	Magnetosheath
N_i (cm^{-3})	2.24 ± 0.26	9.41 ± 1.88	2.90 ± 0.51	14.53 ± 2.51
T_i (eV)	541 ± 95	86 ± 17	721 ± 144	137 ± 34
V_L (km s^{-1})	-16.70 ± 54.09	-193.02 ± 41.53	-42.20 ± 62.59	-265.48 ± 58.47
V_M (km s^{-1})	-8.28 ± 32.19	-13.17 ± 27.92	-13.19 ± 35.68	15.14 ± 18.92
V_N (km s^{-1})	-25.53 ± 29.80	-80.40 ± 23.30	0.16 ± 30.93	4.55 ± 18.98
B_L (nT)	6.63 ± 6.43	15.71 ± 5.64	17.59 ± 4.85	-0.59 ± 15.22
B_M (nT)	12.13 ± 2.22	14.07 ± 4.02	-31.06 ± 4.25	-41.05 ± 5.24
B_N (nT)	-3.63 ± 1.37	-1.04 ± 3.08	-4.77 ± 3.06	-7.88 ± 3.76
$\langle \boldsymbol{B}_{\mathrm{msp}}, \boldsymbol{B}_{\mathrm{msh}} \rangle$[a]	21°.8		30°.1	
$\langle \boldsymbol{B}_{\mathrm{msp}}, \Delta\boldsymbol{V} \rangle$[b]	112°.9		126°.6	
$\langle \boldsymbol{B}_{\mathrm{msh}}, \Delta\boldsymbol{V} \rangle$	134°.7		96°.5	
Wave periods (s)	303 ± 107		266 ± 102	
Phase velocity in LMN (km s^{-1})	$-165.65, -8.08, -69.39$		$-171.06, 3.85, 1.75$	
Wavelength (R_E)	8.5 ± 3.0		7.1 ± 2.7	

Notes.
[a] $\langle \boldsymbol{a}, \boldsymbol{b} \rangle$ denotes the angle between vectors $\boldsymbol{a}$ and $\boldsymbol{b}$.
[b] $\Delta\boldsymbol{V} = \boldsymbol{V}_{\mathrm{msh}} - \boldsymbol{V}_{\mathrm{msp}}$ denotes the velocity shear between the magnetosheath and the magnetosphere.

The boundary conditions are given in Table 1 using the ion and magnetic field data within the magnetosphere and magnetosheath domains. In addition, the angles between $\boldsymbol{B}_{\mathrm{msp}}$, $\boldsymbol{B}_{\mathrm{msh}}$, and velocity shear $\Delta\boldsymbol{V} = \boldsymbol{V}_{\mathrm{msh}} - \boldsymbol{V}_{\mathrm{msp}}$ are given in Table 1. In general, the magnetic shear angles between the magnetosphere and the magnetosheath are 21°.7 and 30°.1 for the K-H waves by *MMS* and *THA*, respectively.

3.3. Properties of K-H Waves

The shapes of the K-H waves on the magnetopause are mostly nonsinusoidal (e.g., Hasegawa et al. 2004; Hwang et al. 2011). The leading (anti-sunward) edges of the magnetopause boundary have steepened shapes, and are widely suggested to be rolled-up during the propagation of the K-H waves (e.g., Nykyri & Otto 2001; Nakamura & Fujimoto 2005). The trailing (sunward) edges are mostly sharp due to the centrifugal force and compression from the magnetosheath flow (Hasegawa et al. 2009). The trailing edges of the K-H waves by *MMS* and *THA* are highlighted by the black vertical lines in Figures 3(a)–(c) and Figures 3(e)–(g). These trailing edges are identified by sharp increases in N_i and V_L, as well as the increases of total (ion plus magnetic) pressure. Altogether 30 ± 3 trailing edges are found within ~2.5 hr in the K-H wave by *MMS*, and 24 ± 2 trailing edges are found within ~1.7 hr in the K-H wave by *THA*. The uncertainties of the numbers come from some ambiguous boundary crossings.

The periods of the K-H waves are estimated by the average periods of all the identified trailing edges, which are 303 ± 107 s and 266 ± 102 s for the K-H waves by *MMS* and *THA*, respectively. Thus, the K-H waves on both flanks have similar wave periods despite their different local times. Figures 3(d) and (h) show the wavelet power spectra of total pressure, which denote that the wave periods vary gradually with time. This can also be implied by the variation of the partial wave periods marked in Figures 3(c) and (g), which are estimated by the average periods of every five adjacent trailing edges. A cross-correlation analysis is performed on the partial wave periods of the trailing edges by *MMS* and *THA*, showing

that the correlation coefficient reaches the maximum when the lag time between the *THA* and *MMS* data is ~18 minutes. Considering the phase speeds of the K-H waves in the *L* direction (~166 km s^{-1} for *MMS* and ~171 km s^{-1} for *THA*; see Table 1) and the distance between the location of *MMS* and the mirror point of the location of *THA* along the magnetopause (~22 R_E), it takes about 13–14 minutes for the K-H waves to propagate from *THA* to *MMS*. The consistency between the lag time and the propagation time suggests that the K-H waves propagate quasi-symmetrically on both flanks. A statistical study by Henry et al. (2017) shows a dawn–dusk asymmetry in the occurrence rates of the K-H instability under Parker-spiral IMF, which can be explained by a larger growth rate at the dawnside (Nykyri 2013). However, K-H waves can be excited simultaneously at both flanks with different growth rates, as is presented in Nykyri's paper and in this case. According to Lin et al. (2014), the wavelengths of the K-H waves are associated with IMF clock angles. It is suggested that the variations of the wavelengths might be modulated simultaneously at the symmetric locations on both flanks by the varying IMF, and roughly preserved during the propagation of the waves due to the dominated plasma dynamic pressure at the low-latitude boundary layer.

The nonlinear evolution of the K-H waves can compress the trailing edges down to ion inertial scale and distort the magnetic fields on both sides of the magnetopause to increase the local magnetic shear, which provides suitable conditions for magnetic reconnection. The recent *MMS* results have discovered the evidence of magnetic reconnection on the trailing edges of the K-H waves (e.g., Eriksson et al. 2016; Li et al. 2016). For the K-H waves in this study, the local magnetic shear angles of the trailing edges are analyzed and compared to the large-scale background magnetic shear on both sides. Figures 4(a) and (b) present two examples of trailing edges observed by *MMS* and *THA*, respectively. The trailing edges are denoted by the vertical dashed lines in each figure. The local magnetic shear angles of the trailing edges are estimated by the angles of the average magnetic fields on the quasi-steady magnetosphere (blue box) and magnetosheath (red box) sides.
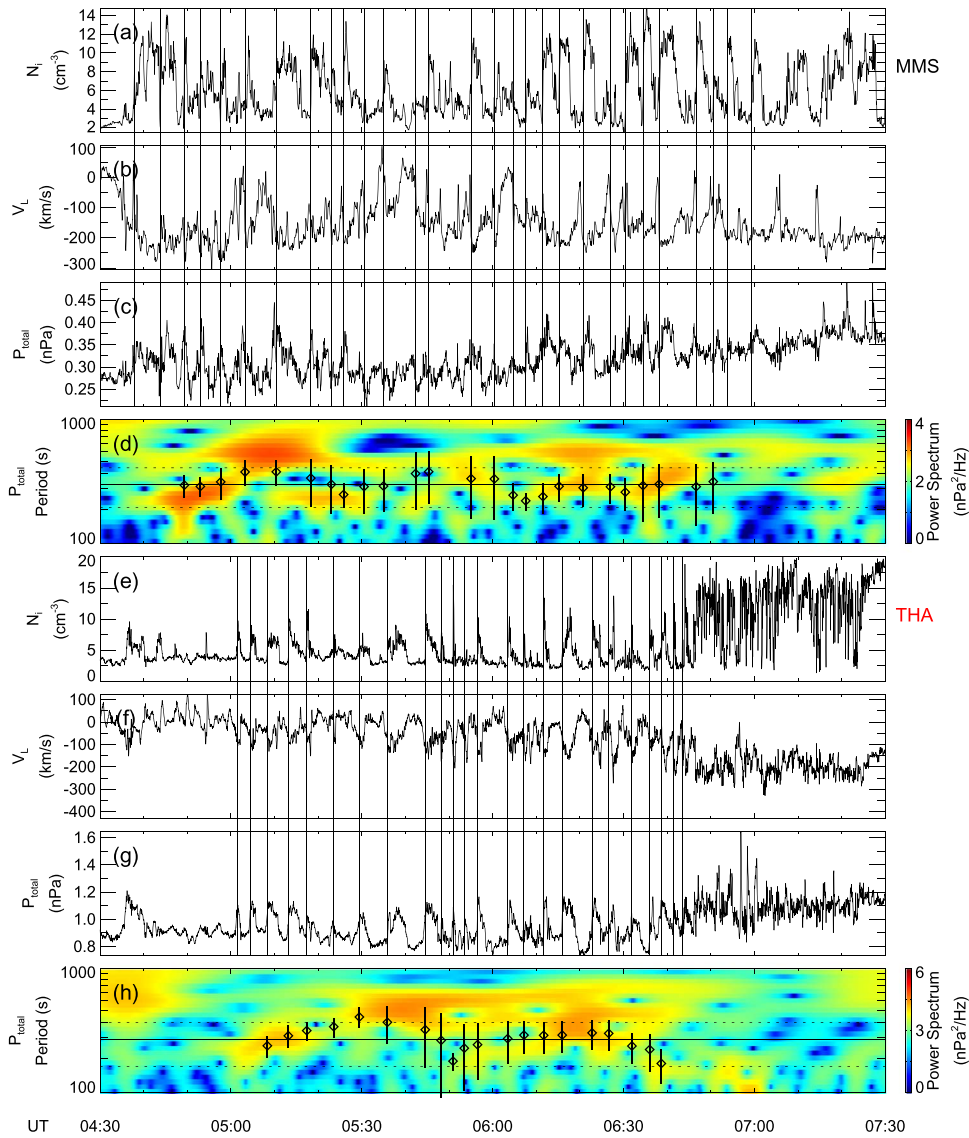
Figure 3. Wave periods of the K-H waves by *MMS* and *THA*. *MMS* observations of (a) N_i, (b) V_L, and (c) total (ion plus magnetic) pressure. The vertical solid lines mark the trailing edges. (d) Wavelet power spectrum of *MMS* total pressure. The horizontal solid line denotes the average time periods of the trailing edges, and the dashed lines denote the errors. The diamonds denote the average values of the periods of every five adjacent trailing edges, and the vertical bars denote the standard deviations of the periods. ((e)–(h)) Analysis of wave periods of the K-H waves by *THA*. These panels are the same as panels (a)–(d).
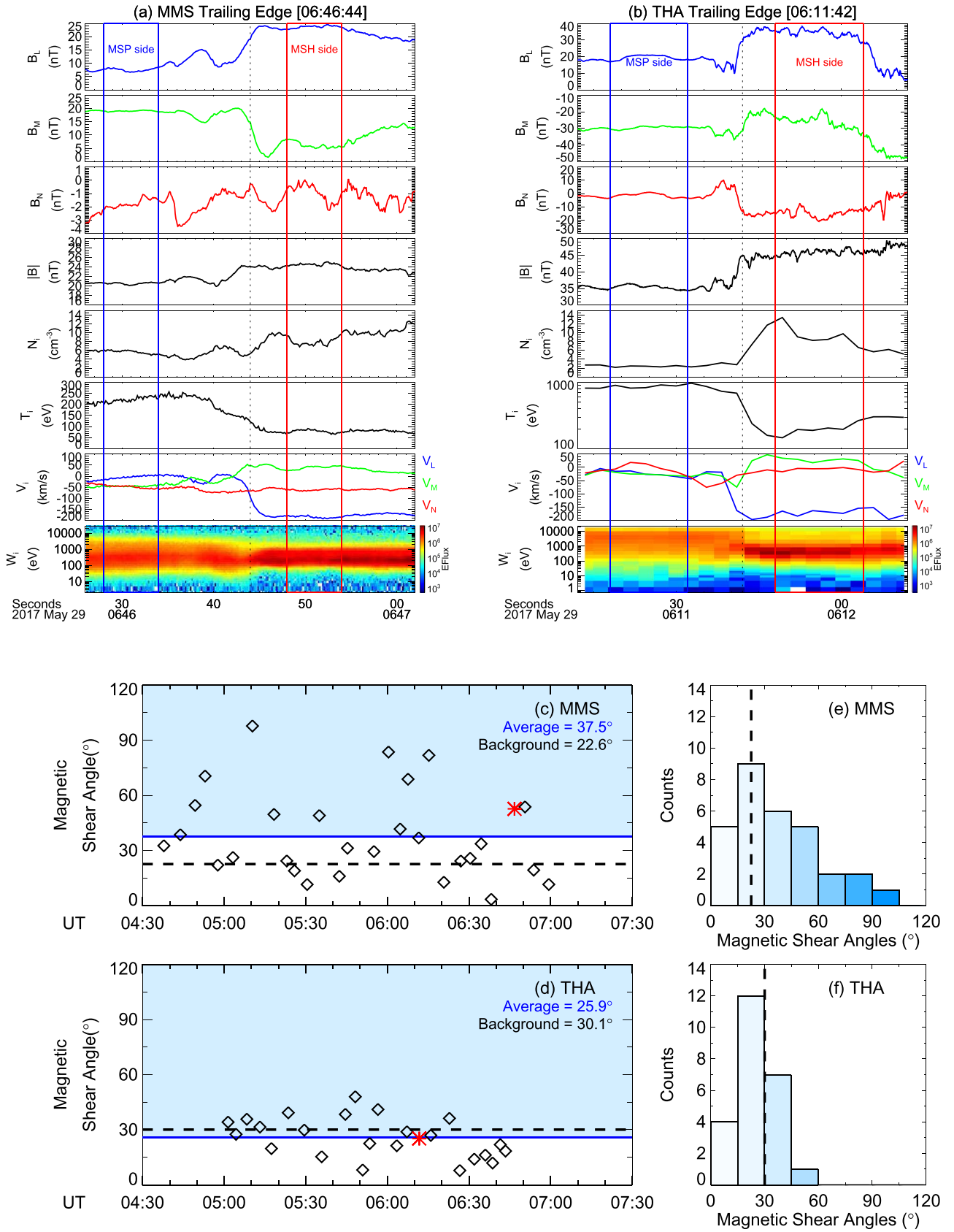
The local magnetic shear angles of the trailing edges shown in Figures 4(a) and (b) are 53°.7 and 25°.2, respectively.

Figures 4(c) and (d) show the local magnetic shear angles for the identified trailing edges. The average local magnetic shear angle of trailing edges observed by *MMS* is 37°.5, which is about 66% larger than the background magnetic shear (22°.5). Comparatively, the average local magnetic shear angle of trailing edges observed by *THA* is 25°.9, which is close to the background magnetic shear (30°.1). The local shear angles of *MMS* trailing edges distribute in a wider range than those of *THA*, in which the largest local shear angle is 98°. The histograms of all the local magnetic shear angles are shown in Figures 4(e) and (f). The results show a trend of stronger magnetic field distortion on the trailing edges during the tailward propagation of the K-H waves. The large magnetic shears on the nightside trailing edges favor the magnetic reconnection, which may transport significant solar wind plasma into the magnetosphere. Some of the *MMS* trailing edges have fast ion flows, which could be the reconnection

outflow (Li et al. 2016). Further studies will analyze the burst-mode data to confirm this.

4. Summary

We report the first simultaneous observations of the Kelvin–Helmholtz waves by *MMS* and *THA* on the dawn and dusk flank magnetopause on 2017 May 29. The solar wind condition is quasi-steady. The solar wind speed is relatively low ($\sim$346 km s^{-1}), and the IMF has a northward B_z and a dominant B_y component. The dawnside K-H waves are observed by *MMS* at [−15.0, −16.3, 3.5] R_E, while the duskside K-H waves are observed by *THEMIS-A* at [3.9, 11.7, −3.7] R_E. The average periods are 303 ± 107 s for the *MMS* K-H wave and 266 ± 102 s for the *THA* K-H wave. The wave periods of the *MMS* and *THA* K-H waves vary gradually on both the dawn and dusk flanks. The variations of wave periods have good correlation when the lag time from *THA* to *MMS* meets the time for propagation of the K-H waves, which

Figure 4. Local magnetic shear angles at the trailing edges of the K-H waves. (a) An example of *MMS* trailing edge at 06:46:44 UT. The blue and red boxes denote the magnetosphere side (06:46:28–06:46:34 UT) and magnetosheath side (06:46:48–06:46:54 UT), respectively. (b) An example of *THA* trailing edge at 06:11:42 UT. The blue and red boxes denote the magnetosphere side (06:11:18–06:11:32 UT) and magnetosheath side (06:11:48–06:12:04 UT), respectively. ((c)–(d)) The local magnetic shear angles of *MMS* and *THA* trailing edges. The red stars denote the trailing edges shown in panels (a) and (b), respectively. The black dashed lines and blue solid lines denote the large-scale magnetic shear angles and the average values of the local magnetic shear angles, respectively. ((e)–(f)) Histograms of the local magnetic shear angles of the *MMS* and *THA* trailing edges. The black dashed lines denote the large-scale magnetic shear angles.

suggests that the evolutions of the K-H waves and the variations of their wave periods are quasi-symmetric on both flanks. The large-scale magnetic shear angles between the magnetosphere and the magnetosheath are 22°.5 for the *MMS* K-H wave and 30°.1 for the *THA* K-H wave. On the trailing edges, *MMS* observed an average local magnetic shear 66% larger than the background magnetic shear, with a maximum local magnetic shear of 98°, while *THA* observed local magnetic shear angles similar to the background magnetic shear. The tailward propagation of the K-H waves distorts the magnetic field on the trailing edges. The significantly increased local magnetic shear favors the magnetic reconnection and plasma transport from the magnetosheath into the magnetosphere.

ORCID iDs

C. T. Russell ⬤ https://orcid.org/0000-0003-1639-8298

References

Angelopoulos, V. 2008, SSRv, 141, 5
Auster, H. U., Glassmeier, K. H., Magnes, W., et al. 2008, SSRv, 141, 235
Borovikov, S. N., & Pogorelov, N. V. 2014, ApJL, 783, L16
Burch, J. L., Moore, T. E., Torbert, R. B., & Giles, B. L. 2015, SSRv, 199, 5
Chandrasekahar, S. 1961, Hydrodynamic and Hydromagnetic Stability (New York: Oxford Univ. Press)
Dimmock, A. P., Nykyri, K., Karimabadi, H., Osmane, A., & Pulkkinen, T. I. 2015, JGRA, 120, 2767
Eriksson, S., Lavraud, B., Wilder, F. D., et al. 2016, GeoRL, 43, 5606
Fairfield, D. H., Kuznetsova, M. M., Mukai, T., et al. 2007, JGRA, 112, A08206
Farrugia, C. J., Gratton, F. T., Bender, L., et al. 1998, JGR, 103, 6703
Farrugia, C. J., Gratton, F. T., Torbert, R. B., et al. 2003, AdSpR, 31, 1105
Foullon, C., Verwichte, E., Nakariakov, V. M., Nykyri, K., & Farrugia, C. J. 2011, ApJL, 729, L8
Guo, X. C., & Wang, C. 2010, JGRA, 115, A01206
Guo, X. C., Wang, C., & Hu, Y. Q. 2010, JGRA, 115, A10218
Hapgood, M. A., & Bryant, D. A. 1992, P&SS, 40, 1431
Hasegawa, H., Fujimoto, M., Phan, T. D., et al. 2004, Natur, 430, 755
Hasegawa, H., Fujimoto, M., Takagi, K., et al. 2006, JGRA, 111, A09203
Hasegawa, H., Retinò, A., Vaivads, A., et al. 2009, JGRA, 114, A12207
Henry, Z. W., Nykyri, K., Moore, T. W., Dimmock, A. P., & Ma, X. 2017, JGRA, 122, 11,888
Hwang, K. J., Kuznetsova, M. M., Sahraoui, F., et al. 2011, JGRA, 116, A08210
Kavosi, S., & Raeder, J. 2015, NatCo, 6, 7019
Li, W., André, M., Khotyaintsev, Y. V., et al. 2016, GeoRL, 43, 5635
Li, W. Y., Guo, X. C., & Wang, C. 2012, JGR, 117, A08230
Li, W. Y., Wang, C., Tang, B. B., Guo, X. C., & Lin, D. 2013, JGRA, 118, 5118
Lin, D., Wang, C., Li, W., et al. 2014, JGRA, 119, 7485
Ling, Y., Shi, Q. Q., Shen, X. C., et al. 2018, JGRA, 123, 3836
McFadden, J. P., Carlson, C. W., Larson, D., et al. 2008, SSRv, 141, 277
Miura, A. 1995, GeoRL, 22, 2993
Nakamura, T. K. M., Daughton, W., Karimabadi, H., & Eriksson, S. 2013, JGRA, 118, 5742
Nakamura, T. K. M., & Fujimoto, M. 2005, GeoRL, 32, L21102
Nakamura, T. K. M., Hasegawa, H., Daughton, W., et al. 2017, NatCo, 8, 1582
Nishino, M. N., Hasegawa, H., Fujimoto, M., et al. 2011, P&SS, 59, 502
Nykyri, K. 2013, JGRA, 118, 5068
Nykyri, K., & Otto, A. 2001, GeoRL, 28, 3565
Otto, A., & Fairfield, D. H. 2000, JGR, 105, 21175
Pollock, C., Moore, T., Jacques, A., et al. 2016, SSRv, 199, 331
Shue, J. H., Chao, J. K., Fu, H. C., et al. 1997, JGR, 102, 9497
Takagi, K., Hashimoto, C., Hasegawa, H., Fujimoto, M., & TanDokoro, R. 2006, JGRA, 111, A08202
Taylor, M. G. G. T., Hasegawa, H., Lavraud, B., et al. 2012, AnGeo, 30, 1025
Terasawa, T., Fujimoto, M., Mukai, T., et al. 1997, GeoRL, 24, 935
Torbert, R. B., Russell, C. T., Magnes, W., et al. 2014, SSRv, 199, 105
Wing, S., Johnson, J. R., Newell, P. T., & Meng, C.-I. 2005, JGRA, 110, A08205
Yan, G. Q., Mozer, F. S., Shen, C., et al. 2014, GeoRL, 41, 4427